sciendo

Polish Journal of Chemical Technology, 20, 2, 85—91, 10.2478/pjct-2018-0027

Synthesis, characterization of Hollandite $Ag_2Mn_8O_{16}$ on TiO_2 nanotubes and their photocatalytic properties for Rhodamine B degradation

Mohamed Thabit, Huiling Liu*, Jian Zhang, Bing Wang

State Key Laboratory of Urban Water Resource and Environment, School of Municipal and Environmental Engineering, Harbin Institute of Technology, 150090 Harbin, China
**Corresponding author: e-mail: hlliu2002@163.com*

In this research $Ag_2Mn_8O_{16}$ nanocrystals/TiO_2 nanotubes, photoelectrodes were successfully prepared through anodization and annihilation steps, followed by electrodeposition of MnO_2 and Ag in a three electrodes cell. The obtained photoelectrodes were dried, then annealed for crystallization, the morphology and structure of the fabricated electrodes were characterized via scanning electron microscopy (SEM), X-ray diffraction (XRD) and X-ray photoelectron spectroscopy (XPS). The light absorption and harvesting properties were investigated through UV–visible diffuse reflectance spectrum (DRS), photocatalytic performances were evaluated by degradation of 50 mL of Rhodamine B (5 mg L_{-1}) under Xenon light irradiation for 2 h. Results illustrated that the fabricated photoelectrodes show remarkable photo-degradation properties of organic pollutants in aqueous mediums.

Keywords: Ag-MnO_2/TiO_2, $Ag_2Mn_8O_{16}$, nanotubes, nanocrystals, Photoelectrode, electrochemical deposition, Rhodamine B, Photo-catalytic efficiency.

INTRODUCTION

In the past decades the technology of one dimensional Titanium dioxide (TiO_2) nano-material structures, such as nanotubes, nanoflakes, nanorods and nanowires[1–4] have attracted significant attention due to their remarkable advantages such as nontoxicity, high stability, natural power resources, photo-catalytic capabilities, and also because of the high cost of noble metal oxide catalysts[4, 5]. TiO_2 has been studied as a cheap alternative metal oxide catalyst for water oxidation that can be used to degrade various types of water pollutants. It is considered revolutionary since the discovery of water splitting on the TiO_2 surface due to its remarkable photo-catalytic capabilities6. However, the tubular structure caught attention due to its superior light harvesting properties and large internal surface area[7–9]. From this point, a number of semiconductors, such as Pd, Ru, Cd, etc., were found to enhance the Titanium dioxide nanotube arrays catalytic performance10. These electrochemical capacitors with their high power density, long cycling life time, and fulfilling the power and energy gap between traditional dielectric capacitors and batteries[11, 12], showed MnO_2 to be a promising pseudocapacitive material with high theoretical specific capacitance – in the order of 1400 F g^{-1}. A previous report has shown that MnO_x can improve the absorption of visible-light and facilitate the separation of the electron-hole pairs, because of its low charge transfer resistance and multitudinous defects[13–15], which can show considerably enhanced oxygen evolution reaction (OER) activity as a non-noble catalyst. Several studies on MnO_2 itself, as a catalyst for OER of water, have been performed[16, 17].Nanoscale MnO_2 was prepared and incorporated into electrically conductive frameworks, which has been well proven to be an effective and promising strategy. Developing nanostructured current collectors with the high surface area and enhanced conductivity is also mandatory for supercapacitor materials[18–20], however, more enhancement is required to achieve the remarkable photocatalytic properties of the MnO_x/TiO_2 photoelectrodes[21]. There have been quite a few types of research researcher concerning Ag-TiO_2 nanocomposites used as photoactive materials[22–24] in many photoactive applications due to their localized surface plasmon resonance characteristics. Moreover, Ag exhibited the lowest sheet resistance (30 Ω sq^{-1}) and highest transmittance (90%) in the 500–700 nm region[25–27]. Silver deposits on TiO_2 have been shown to enhance the mineralization of mono-, di-poly-carboxylic acids, and the removal of 2-propanol, chloroform, and urea[28–31]. Herein, we report the fabrication of Ag-MnO_2/TiO_2 NTs photoelectrodes which led to formatting $Ag_2Mn_8O_{16}$ NCs/TiO_2 NTs via annihilation and then we investigated their photocatalytic performance. The experimental results show that the nanocrystals show excellent photocatalytic properties for degradation of toxic organic and textile dyes, however, electrocatalytic activity is not investigated due to the effect of the electric current on the stability of the deposited materials structure.
MATERIALS AND METHODS

Material

All chemicals used in this study were analytical grade and were employed without further purification. Titanium sheets were purchased from Baoji and Baoye Titanium–Nickel Manufacturing Co., Ltd. Sodium sulfate (Na_2SO_4), Ammonium Fluoride (NH_4F), acetone, absolute ethanol, potassium permanganate ($KMnO_4$), Silver nitrate ($AgNO_3$), Rhodamine B(RhB), Power supply 0 to 30 V electric potential and 0 to 5A electric current. Magnetic agitators, 35 W xenon light source, 50 x 60 x 40 cm light isolation metal box.

Photoelectrode Preparation

The size of the strip titanium sheet is 90 mm × 10 mm × 0.5 mm. The effective work area is 40 mm × 10 mm × 0.5 mm, the titanium foils were cleaned by immersing them in a mixture of acetone and absolute ethanol, then in an ultrasonic water bath for 30 minutes, the foils were left to dry for 1 hour at 80°C in a vacuum oven. After completely drying the foils, they were immersed in a mixture of (HF: HNO_3: H_2O = 1:4:5 in volume)

for 30 seconds, followed by rinsing with D.I water, then drying in a vacuum oven for 4 hours at 70°C.

The polished titanium foils were anodized at a constant potential of 20 V in a mixture of 1M Sodium sulfate (Na_2SO_4), containing 0.5%wt Ammonium Fluoride (NH_4F) solution, at 40°C for 2 h in a two-electrode configuration with a platinum cathode, After anodic oxidation, the samples were rinsed with deionized water and dried in air, the resulting amorphous TiO_2 NTs were annealed at 500°C for 2 h with heating and cooling rates of 2°C min^{-1} in air to crystallize the tubes.

Preparation of $Ag_2Mn_8O_{16}$ NC/TiO_2 NTAs Photo-electrode

The $Ag_2Mn_8O_{16}$ NC/TiO_2 nanotube arrays photo-electrodes were prepared via two steps of electro deposition. At first MnO_2 particles were deposited onto the surface of previously prepared bare TiO_2 NTAs; the deposition of the MnO_2 process was conducted in the solution of $KMnO_4$ (0.2 mol/L) for 8 min. The electrochemical deposition was performed using a two-electrode system with the prepared TiO_2 NTAs foil as electrode and platinum foil as the counter electrode. The electro-depositions were carried out at a constant current of 10 mA for 10 to 15 minutes at room temperature. The deposition solution was constantly stirred at 150 rpm during the process. MnO_2/TiO_2 NTs photoelectrodes were obtained after natural drying and annealing at 500 C for 1 hour, and afterwards the Ag particles were electro-deposited onto the surface of the prepared MnO_2/TiO_2-NTs electrodes by the galvanostatic method, using a three-electrode system with the MnO_2/TiO_2 NTs as the working electrode, a Pt counter electrode, and Ag/AgCl (3 M KCl) reference electrode. The galvanostatic deposition was carried out at 0.3 mA for 10 minutes in an aqueous solution containing 0.75 mM $AgNO_3$. After the electro-deposition process, the Photo-electrodes were washed with distilled water and then dried in a vacuum oven at 80°C for 4 hours.

RESULTS AND DISCUSSIONS

Photoelectrodes Characterization

SEM Analysis

An SEM test was performed on as-prepared, bare-TiO_2 nanotubes sample and the $Ag_2Mn_8O_{16}$ nanocrystals/TiO_2 nanotubes Photoelectrode. The results shown in Figure 1A illustrated the typical tubular structure with an average diameter of 100 nm and an average wall thickness of 20 nm, while scanning samples, obtained after 1∼2 minutes of the second electrodeposition process, showed the crystalline formation in and onto the surface of TiO_2 nanotubes, as shown in Figure 1B. The SEM scanning results of the final product showed that the modified TiO_2 nanotubes were completely covered with nanocrystals. The obtained field emission scanning electron microscope images showed a hexagonal prismatic crystalline structure, Figure 1C.Which corresponds to the well-known hollandite crystals structure[32–34], where the obtained crystals possess an average diameter of 30 nm and length over 200 nm.

Thus, X-ray diffraction and X-ray photoelectron spectroscopy tests were essential to clarify the properties and the elemental composition of the formatted crystals shown in the obtained SEM images.

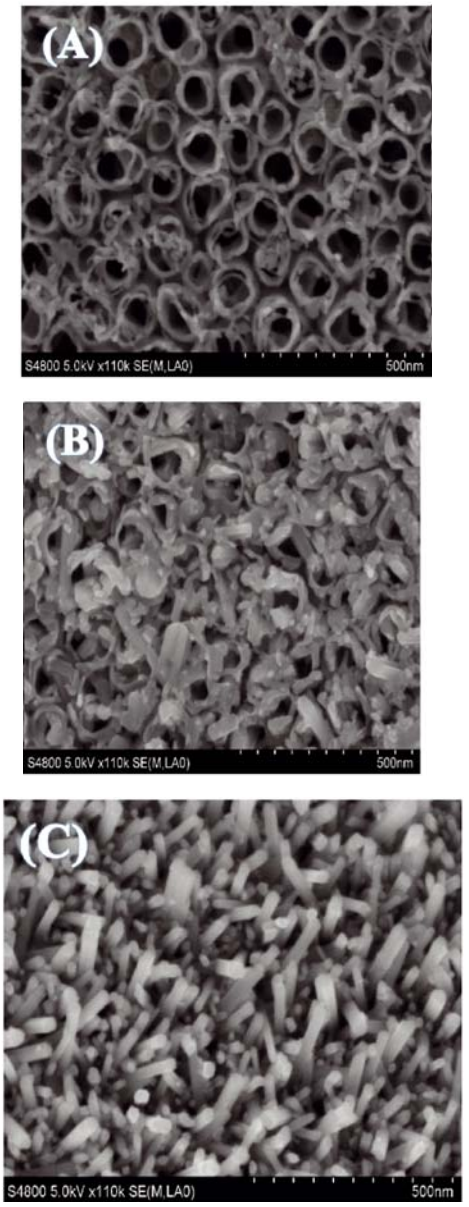

Figure 1. (A) SEM image of bare TiO_2 NTAs, (B) $Ag_2Mn_8O_{16}$ NCs formation onto TiO_2 nanotubes (C) $Ag_2Mn_8O_{16}$ NCs/TiO_2 NTAs photoelectrodes

XRD analysis

X-ray diffraction (XRD) was performed on a D8 Advance (Bruker) diffractometer with Cu K radiation. The accelerating voltage and applied current were held at 40 kV and 30 mA, respectively. Ultraviolet-visible diffuse reflectance spectroscopy (UV–vis DRS) was recorded on a TU-1901 spectrophotometer equipped with an integrating sphere, in which $BaSO_4$ was used as the reflectance sample. The XRD patterns of bare TiO_2 NTAs, MnO_2/TiO_2 NTAs, and $Ag_2M_{n8}O_{16}$ NCs/TiO_2 NTAs samples were performed and are shown in Figure 2. The diffraction peaks are observed at 2Θ = 25.41°, 28.66°, 37.56°, 40.26°, 41.95°, 63.04°, 70.748° and 76.32° which correspond to the (101), (310), (211), (101), (301), (102), (110), (103) and (112) planes, respectively. Clearly, all the crystallite phase could be indexed from their corresponding characteristic peaks, The polymorphic modification of TiO_2 at 500°C are indexed as (101) and (103) planes which

display the phase of anatase crystallization, while (110) plane displays the rutile crystallization. After decoration with the MnO_2 NCs/ TiO_2 NTAs and $Ag_2Mn_8O_{16}$ NCs / TiO_2 samples exhibited three additional diffraction peaks located at 28.66° and 41.95°, corresponding to the transformation of MnO_2 to hexagonal phase(310), and (301) of $Ag_2Mn_8O_{16}$ NCs, which are in coordination with the peaks cited in the literature.

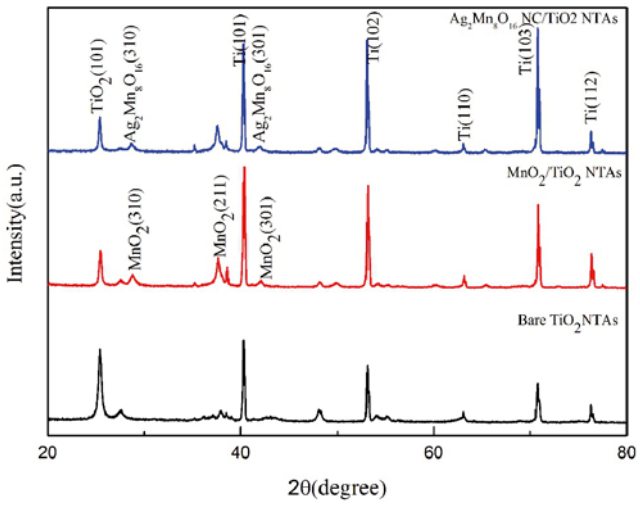

Figure 2. XRD patterns of bare TiO_2 NTAs, MnO_2/TiO_2 NTAs, and $Ag_2Mn_8O_{16}$ NCs/TiO_2 NTAs photoelectrodes

DRS analysis

In order to investigate the visible light absorption capabilities of the fabricated Photoelectrode, UV–vis DRS analysis was performed on both bare TiO_2 NTAs, MnO_2/TiO_2 NTAs and $Ag_2Mn_8O_{16}$ NCs/TiO_2 NTAs photoelectrodes. Bare TiO_2 NTAs samples exhibited typical UV and visible light absorption ratios, while the light absorbance edge of $Ag_2Mn_8O_{16}$ NCs/TiO_2 NTAs photoelectrodes was significantly shifted to the visible region, with the strongest peak located between 400 and 700 nm with a higher absorbance ratio, as shown in Figure 3. Moreover, the mentioned photoelectrodes samples exhibited a typical onset absorption edge, at about 360 nm, corresponding to the electronic transition from O2− anti-bonding orbital to the lowest empty orbital of Ti4+ (O2p → Ti3d)[35].

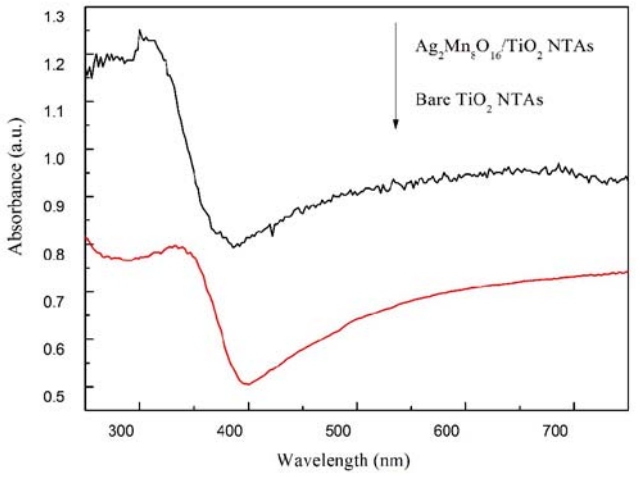

Figure 3. DRS analysis of bare TiO_2 NTAs, MnO_2/TiO_2 NTAs and $Ag_2Mn_8O_{16}$ NCs/TiO_2 NTAs photoelectrodes

Thus, the $Ag_2Mn_8O_{16}$ NCs/TiO_2 NTAs photoelectrodes significant absorbance shift to visible light can only be attributed to the coating of $Ag_2Mn_8O_{16}$ hexagonal nanocrystals, furthermore, the band gap of TiO_2 NTAs could be calculated through the following Kubelka–Munk equation[36, 37].

$$\alpha h\nu = A(h\nu - E_g)^n$$

Where ν, α, Eg, and A are the absorption coefficient, light frequency, band gap, and constant, respectively. Among them, n depends on the characteristics of the transition in a semiconductor, such as direct transition where n=1 or indirect transition where n=4. Thus, from the results obtained in the DRS analysis, the photon energy (hν) is estimated via the photon energy model equation, hν = 1240/λ (the wavelength), while $(\alpha h\nu)^2$ = (photon energy (hν) x absorbance value)^2.

The optical band gap of $Ag_2Mn_8O_{16}$ NCs/TiO_2 can be determined from the plot of $(\alpha h\nu)^2$ as a function of hν by extrapolating the linear portion of the curve to intersect the photon energy axis at zero absorption. The plots: α versus λ (the wavelength), and $(\alpha h\nu)^2$ versus hν, as well as the extrapolated direct allowed band gap Eg values are shown in Figure 4.

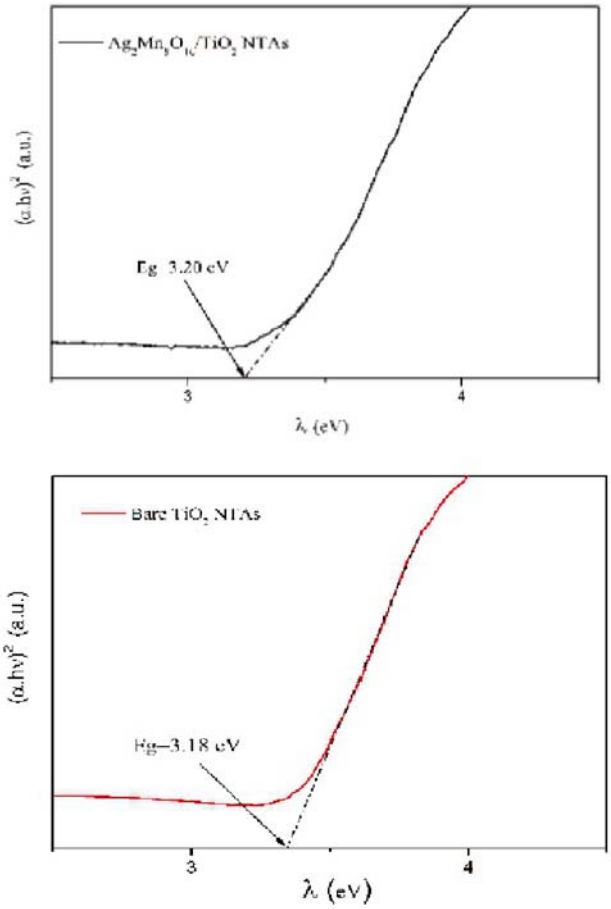

Figure 4. Plots of $(\alpha \cdot h\nu)^2$ vs. hν of TiO_2 NTAs and $Ag_2Mn_8O_{16}$ /TiO_2 NTAs determined band gap energy (Eg)

The estimated Eg value of band gap of TiO_2 NTAs and $Ag_2Mn_8O_{16}$ /TiO_2 NTAs were found to be 3.18 and 3.20 eV, respectively. Accordingly, the fabricated photo-electrodes can absorb and make use of both UV (290–400 nm) and visible (400–700 nm) radiation to enhance process efficiencies.

XPS analysis

To investigate the existence of the electrodeposited elements on the surface of the fabricated photoelectrode, XPS analysis was made use of to survey the existence of elements on the photoelectrode as a result of the electrochemical process, as shown in Figure 5A, and to characterize the chemical species of the discovered elements.

The existence of Manganese elements can be determined by observing the Mn 2p peaks located between 640 eV and 660 eV. The results show Mn 2p1/2 and Mn 2p3/2 peaks at 640.33 and 652.28 eV respectively, as shown in Figure 5B, which attribute to the presence of two Manganese (Mn) valances, Mn_2O_3 and MnO_2, the oxidation state of manganese can be determined by using the known oxidation state of oxygen and the overall charge of the ion, the oxidation state in manganese(III) oxide (Mn_2O_3) is Mn^{+3} and the oxidation state in manganese dioxide(MnO_2) is Mn^{+2}. Thus, from the obtained results the oxidation state of manganese in $Ag_2Mn_8O_{16}$ is $Mn^{+15/4}$, while the XPS spectra of Ag 3d is given. From the literature, we know that there are two silver species, metallic Ag, and Ag_2O; each silver species showed two peaks, owing to the Ag 3d5/2 and Ag 3d3/2 transition. The Ag peaks are centered at 367.7 eV and 373.8 eV , as shown in Figure 5C, which contributes to the presence of Ag_2O as found in the literature[38, 39], and in accordance to the XRD results shown in Figure 2 and as a part of the $Ag_2Mn_8O_{16}$ structure.

Rhodamine B degradation performance

Rhodamine B (RhB) has been widely employed as a dye, especially for textile and industrial dyes. RhB molecules were often chosen as a representative pollutant to evaluate the PC performance of the as-synthesized catalysts. Thus, in this research, the degradation of RhB was used to evaluate the PC performances of the as-constructed $Ag_2Mn_8O_{16}$ NCs/TiO_2 NTAs photoelectrodes.

Thus, the photodegradation efficiency (DE) was estimated according to the following equation[40]:

$$DE = \frac{C_0 - C_t}{C_0} \times 100$$

The results of the photodegradation process have shown a remarkable degradation efficiency superior to the degradation by Ag/TiO_2 and MnO_2, the degradation ratios of the three photoelectrodes are ranged in this order: $Ag_2Mn_8O_{16}$ NCs/TiO_2 NTs> Ag/TiO_2 NTs>MnO_2 NTs, as illustrated in Figure 6.

Therefore, the high-efficiency ratio can only be attributed to the formation of $Ag_2Mn_8O_{16}$ nanocrystals onto the TiO_2 NTs photoelectrode, which contributed to the photodegradation efficiency of RhB due to the high production rate of ·OH and·O2 radicals. The degradation ratio of RhB was estimated via the pseudo-first-order kinetics function, according to the Langmuir–Hinshelwood (L-H) model[41]:

The Kinetic linear fitting curves of photocatalytic degradation, shown in Figure 7, illustrate the superior

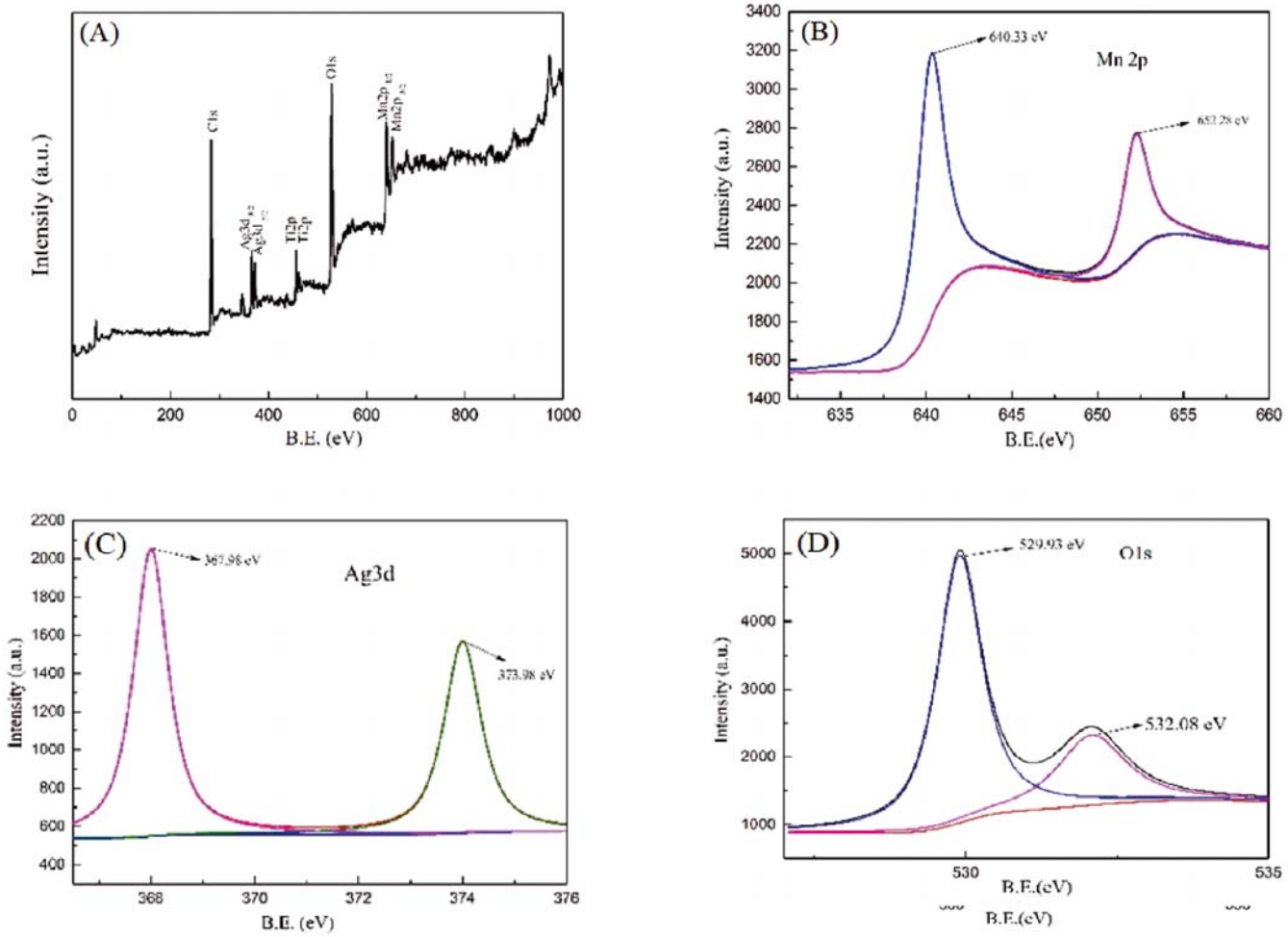

Figure 5. XPS spectra diagram of (A) survey spectra, (B) Mn 2p, (C) Ag 3d and (D) O 1s

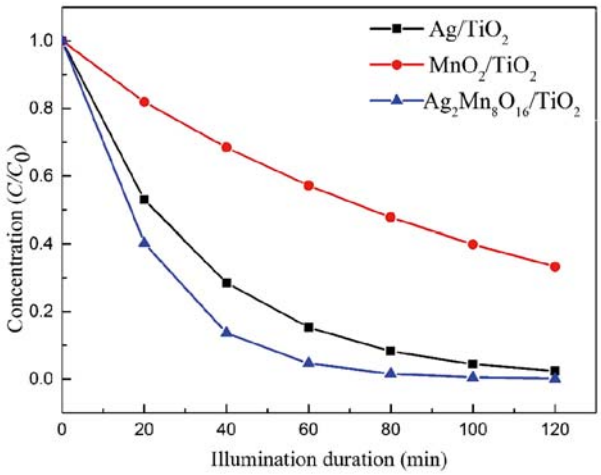

Figure 6. Rhodamine B Degradation ratio during the illumination process

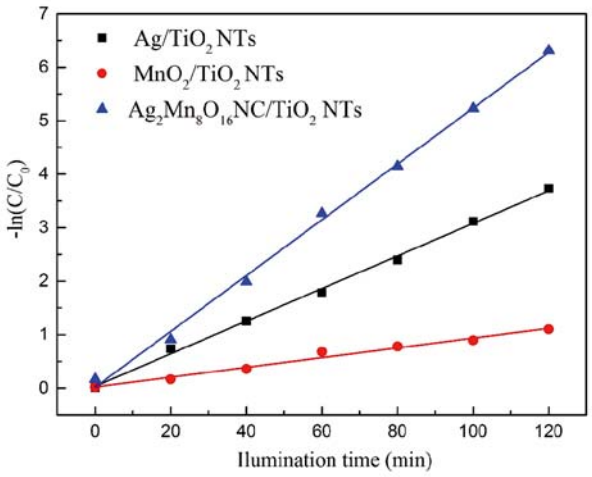

Figure 7. Kinetic linear fitting curves of photocatalytic degradation of RhB by $Ag_2Mn_8O_{16}$ NCs/TiO_2 NTs, Ag/TiO_2 NTs, and MnO_2/TiO_2 NTs

photocatalytic performance of the $Ag_2Mn_8O_{16}$ NCs/TiO_2 NTs over the Ag/TiO_2 NTs and MnO_2 NTs. It can be deduced that $Ag_2Mn_8O_{16}$ NCs/TiO_2 NTs photoanode displays PC activity with the rate constant of 0.0522 min^{-1} under Xenon light irradiation.

The result shows that the photocatalytic degradation of Rhodamine B of these samples can be described by the first order kinetic model, as mentioned above. The linear relationship with the irradiation time, the calculated rate constants and the correlation coefficients corresponding are as listed in Table 1.

The ability to reapply salvaged photoelectrodes is important for their practical application. This was determined via a stability test. The concentration and stability of the solution of the designated organic pollutant (Rhodamine B) were stored in the dark and saved in black agar containers. Before administering the photodegradation process, the mixture is agitated for 20 minutes inside an isolated metal box to reach a state of adsorption-desorption equilibrium. Afterwards, the $Ag_2Mn_8O_{16}$ NCs/TiO_2 NTs Photoelectrode is placed inside a photoreactor filled with 50 mL of Rhodamine B solution and illuminated for 2 h. The process was repeated for seven successive-cycles and samples were collected after 20, 40, 60 and 120 min of illumination and tested within each cycle. The results show that the catalyst exhibited catalytic performance without any significant deactivation, revealing its high stability after multiple scavenging processes. There is no significant difference between the performance of the photoelectrode at the first cycle and the last one, and the degradation ratio deference is approximate – (0.2%–0.8%). The stability results are shown in Figure 8.

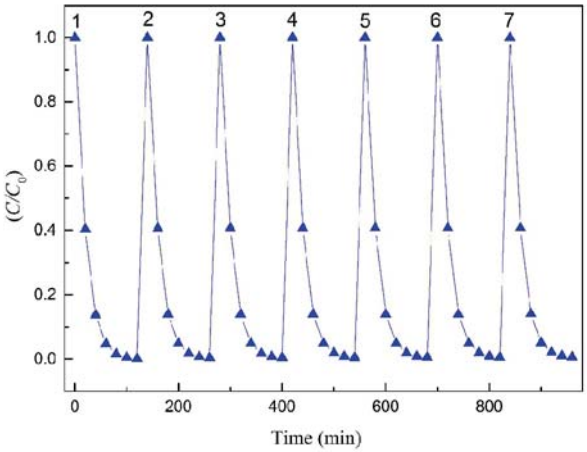

Figure 8. Photocatalyst stability test of prepared $Ag_2Mn_8O_{16}$ NCs/TiO_2 NTAs photoelectrodes

CONCLUSION

$Ag_2Mn_8O_{16}$ nanocrystals were formatted onto the surface of the TiO_2 nanotubes photo-electrodes during the attempt to fabricate Ag-MnO_2/TiO_2 photo-electrodes. The obtained electrodes were examined via several tests. By means of Scanning Electron Microscopy (SEM) the hexagonal prismatic shape of the crystals was viewed, while an X-ray diffraction (XRD) test illustrated the formatted crystals composition, and these crystals were found to be $Ag_2Mn_8O_{16}$ nanocrystals. A further XPS scan was performed on the surface of the fabricated photoelectrode to certify the existence of the deposited elements. $Ag_2Mn_8O_{16}$ nanocrystals are known for their electro catalytic capabilities, especially in the field of lithium-air batteries. In this research, the photocatalytic capabilities of $Ag_2Mn_8O_{16}$ NCs/TiO_2 NTs were tested by means of a DRS test and Rhodamine B photo degradation. The obtained results have shown enhanced photocatalytic properties in both tests, and the overall photo-degradation ratio of Rhodamine B was found satisfactory, and clarified that $Ag_2Mn_8O_{16}$ NCs/TiO_2

Table 1. Photoelectrocatalytic degradation kinetics of Rhodamine B using $Ag_2Mn_8O_{16}$ NCs/TiO_2 NTs, Ag/TiO_2 NTs and MnO_2/TiO_2 NTs Photoelectrode

Samples	First order reaction kinetics equation	Apparent rate constants [k]	Correlation coefficient [R^2]
$Ag_2Mn_8O_{16}$ NC/TiO_2 NTs	y = 0.0522x + 0.0164	0.0522	0.9974
MnO_2/TiO_2 NTs	y = 0.0091x + 0.0237	0.0091	0.9977
Ag/TiO_2 NTs	y = 0.0305x + 0.0343	0.0305	0.9909

nanotubes photoelectrodes are suitable candidates for water organic pollutants' degradation. In addition, it is essential to mention that MnO_2/TiO_2 NTs photo--electrodes exhibited poor photocatalytic properties in comparison with noble elements, such as Cd, Pd, Au, Ag, etc., therefore their photocatalytic performance was neglected. However, when combined with a noble element as one semiconductor, it improves the electron transfer, which enhances the photodegradation performance of the prepared photoelectrodes.

ACKNOWLEDGMENTS

This work was supported by the National Natural Science Foundation of China (51178138), the National Creative Research Groups of China (51121062) and the State Key Laboratory of Urban Water Resources and Environment (2010DX03).

LITERATURE CITED

1. Chen, Q., Liu, H., Xin, Y., Cheng, X., Zhang, J., Li, J., Wang, P. & Li, H. (2013). Controlled anodic growth of TiO_2 nanobelts and assessment of photoelectrochemical and photocatalytic properties. *Electrochim. Acta.* 99, 152–160. DOI: 10.1016/j.electacta.2013.03.032.

2. Cheng, X., Liu, H., Chen, Q., Li, J. & Wang, P. (2013). Construction of N, S codoped TiO_2 NCs decorated TiO_2 nano-tube array photoelectrode and its enhanced visible light photocatalytic mechanism. *Electrochim. Acta.* 103, 134–142. DOI: 10.1016/j.electacta.2013.04.072.

3. Yao, Y., Li, K., Chen, S., Jia, J., Wang, Y. & Wang, H. (2012). Decolorization of hodamine B in a thin-film photo-electrocatalytic (PEC) reactor with slant-placed TiO_2 nano-tubes electrode. *J. Chem. Eng.* 187, 29–35. DOI: 10.1016/j.cej.2012.01.056.

4. Sun, S., Chen, C., Sun, J., Peng, Q., Lü, K. & Deng, K. (2013). Enhancement of catalytic degradation of Rhodamine B under sunlight with Au loading TiO_2 nanotube arrays. *J. Procedia Environ. Sci.* 18, 620–624. DOI: 10.1016/j.proenv.2013.04.085.

5. Cheng, X., Liu, H., Chen, Q., Li, J. & Wang, P. (2013). Preparation and characterization of palladium nano-crystallite decorated TiO_2 nano-tubes photoelectrode and its enhanced photocatalytic efficiency for degradation of Diclofenac. *J. Hazard. Mater.* 254, 141–148. DOI: 10.1016/j.jhazmat.2013.03.062 .

6. Yu, X., Zhang, Y. & Cheng, X. (2014). Preparation and photoelectrochemical performance of expanded graphite/TiO_2 composite. *Electrochim. Acta*. 137, 668–675. DOI: 10.1016/j.electacta.2014.06.027.

7. Zhong, H., Shaogui, Y., Yongming, J. & Cheng, S. (2009). Microwave photocatalytic degradation of Rhodamine B using TiO_2 supported on activated carbon: Mechanism implication. *J. Environ. Sci.* 21(2), 268–272. DOI: 10.1016/S1001-0742(08)62262-7.

8. Fan, M., Hu, S., Ren, B., Wang, J. & Jing, X. (2013). Synthesis of nanocomposite TiO_2 /ZrO_2 prepared by different templates and photocatalytic properties for the photodegradation of Rhodamine B. *J. Powder Technol.* 235, 27–32. DOI: 10.1016/j.powtec.2012.09.042.

9. Cheng, X., Pan, G. & Yu, X. (2015). Visible light responsive photoassisted electrocatalytic system based on CdS NCs decorated TiO_2 nano-tube photoanode and activated carbon containing cathode for wastewater treatment. *Electrochim. Acta.* 156, 94–101. DOI:10.1016/j.electacta.2015.01.042

10. Chen, Q., Liu, H., Xin, Y. & Cheng, X. (2013). TiO_2 nanobelts–effect of calcination temperature on optical, photoelectrochemical and photocatalytic properties. *Electrochim. Acta.* 111, 284–291. DOI: 10.1016/j.electacta.2013.08.049.

11. Cheng, X., Yu, X. & Xing, Z. (2013). Synthesis and characterization of C–N–S tridoped TiO_2 nano-crystalline photocatalyst and its photocatalytic activity for degradation of Rhodamine B. *J. Phys. Chem. Solids* 74(5), 684–690. DOI: 10.1016/j.jpcs.2013.01.004.

12. Zhang, J., Liu, H., Wang, B., Thabit, M. & Bai, H. (2015). Preparation of Pd/Go/Ti electrode and its electrochemical degradation for 2, 4-dichlorophenol. Materials & Design. 86, 664–669. DOI: 10.1016/j.matdes.2015.07.146.

13. Hu, J., Jiang, N., Li, J., Shang, K., Lu, N. & Wu, Y. (2016). Degradation of benzene by bipolar pulsed series surface/packed-bed discharge reactor over MnO_2 –TiO_2 /zeolite catalyst. *Chem. Engine. J*. 293, 216–224. DOI: 10.1016/j.cej.2016.02.036.

14. Luo, S., Zhou, W., Xie, A., Wu, F., Yao, C., Li, X., Zuo, S. & Liu, T. (2016). Effect of mno 2 polymorphs structure on the selective catalytic reduction of NO_x with NH_3 over TiO_2 –palygorskite. *Chem. Engine. J* 286, 291–299. DOI: 10.1016/j.cej.2015.10.079.

15. Huang, Y.G., Zhang, X.H., Chen, X.B., Wang, H.Q., Chen, J.R., Zhong, X.X. & Li, Q.Y. (2015). Electrochemical properties of MnO_2 -deposited TiO_2 nanotube arrays 3d composite electrode for supercapacitors. *Int. J. Hydrogen Energy.* 40(41), 14331–14337. DOI: 10.1016/j.ijhydene.2015.05.014.

16. Guo, X.L., Kuang, M., Li, F., Liu, X.Y., Zhang, Y.X., Dong, F. & Losic, D. (2016). Engineering of three dimensional (3-d) diatom@TiO_2 @MnO_2 composites with enhanced supercapacitor performance. *Electrochim. Acta*. 190, 159–167. DOI: 10.1016/j.electacta.2015.12.178.

17. Ramesh, M., Nagaraja, H.S., Rao, M.P., Anandan, S. & Huang, N.M. (2016). Fabrication, characterization and catalytic activity of α-MnO_2 nanowires for dye degradation of reactive black 5. *Mater. Lett.* 172, 85–89. DOI: 10.1016/j.matlet.2016.02.076.

18. Zhou, H., Zou, X. & Zhang, Y. (2016). Fabrication of TiO_2 @MnO_2 nanotube arrays by pulsed electrodeposition and their application for high-performance supercapacitors. *Electrochim. Acta.* 192, 259–267. DOI: 10.1016/j.electacta.2016.01.182.

19. Cetinkaya, T., Tokur, M., Ozcan, S., Uysal, M. & Akbulut, H. (2016). Graphene supported α-MnO_2 nanocomposite cathodes for lithium ion batteries. *Int. J. Hydrogen Energy.* 41(16), 6945–6953. DOI: 10.1016/j.ijhydene.2015.12.092.

20. Yang, Y., Zhou, Y. & Wang, T. (2014). Preparation of optically active polyurethane/TiO_2 /MnO_2 multilayered nanorods for low infrared emissivity. Mater. Lett. 133(10), 269–273. DOI: 10.1016/j.matlet.2014.06.184.

21. Ma, Z. & Zhao, T. (2016). Reduced graphene oxide anchored with MnO_2 nanorods as anode for high rate and long cycle lithium ion batteries. *Electrochim. Acta*. 201, 165–171. DOI: 10.1016/j.electacta.2016.03.200.

22. Junlabhut, P., Boonruang, S., Mekprasart, W. & Pecharapa, W. (2016). Ag nanoparticle-doped SiO_2 /TiO_2 hybrid optical sensitive thin film for optical element applications. Surface & Coatings Technology. 306, 262–266. DOI: 10.1016/j.surfcoat.2016.06.033.

23. Hussain, M., Tariq, S., Ahmad, M., Sun, H., Maaz, K., Ali, G., Hussain, S.Z., Iqbal, M., Karim, S. & Nisar, A. (2016). Ag TiO_2 nanocomposite for environmental and sensing applications. Materials Chemistry & Physics. 181, 194–203. DOI: 10.1016/j.matchemphys.2016.06.049.

24. Kim, J.H., Kim, D.H., Kim, S.K., Bae, D., Yoo, Y.Z. & Seong, T.Y. (2016). Control of refractive index by annealing to achieve high figure of merit for TiO_2 /Ag/TiO_2 multilayer films. Ceram. Int. 42(12), 14071–14076. DOI: 10.1016/j.ceramint.2016.06.015.

25. Khosravani, S., Dehaghi, S.B., Askari, M.B. & Khodadadi, M. (2016). The effect of various oxidation temperatures on structure of Ag-TiO_2 thin film. Microelectron. Eng. 163, 67–77. DOI: 10.1016/j.mee.2016.06.008.

26. Zhao, Z., Sun, J., Xing, S., Liu, D., Zhang, G., Bai, L. & Jiang, B. (2016). Enhanced raman scattering and photocatalytic

activity of TiO_2 films with embedded ag nanoparticles deposited by magnetron sputtering. Journal of Alloys & Compounds. 679, 88–93. DOI: 10.1016/j.jallcom.2016.03.248.

27. Kuo, D.H., Hsu, W.T. & Yang, Y.Y. (2016). From the fluorescent lamp-induced bactericidal performance of sputtered Ag/TiO_2 films to re-explore the photocatalytic mechanism. Applied Catalysis B Environmental. 184(1), 191–200. DOI: 10.1016/j.apcatb.2015.11.032.

28. Wang, X., Zhao, Z., Ou, D., Tu, B., Cui, D., Wei, X. & Cheng, M. (2016). Highly active Ag clusters stabilized on TiO_2 nanocrystals for catalytic reduction of p -nitrophenol. *Appl. Surf. Sci.* 385, 445–452. DOI: 10.1016/j.apsusc.2016.05.147.

29. Zhong, J.S., Wang, Q.Y., Zhang, M., Chen, D.Q. & Ji, Z.G. (2016). In situ fabrication of TiO_2 nanotube arrays sensitized by Ag nanoparticles for enhanced photoelectrochemical performance. Mater. Lett. 182, 163–167. DOI: 10.1016/j.matlet.2016.06.102.

30. Nasrollahzadeh, M., Atarod, M., Jaleh, B. & Gandomirouzbahani, M. (2016). In situ green synthesis of Ag nanoparticles on graphene oxide/TiO_2 nanocomposite and their catalytic activity for the reduction of 4-nitrophenol, congo red and methylene blue. Ceram. Int. 42(7), 8587–8596. DOI: 10.1016/j.ceramint.2016.02.088.

31. Rismanchian, A., Chen, Y.W. & Chuang, S.S.C. (2016). In situ infrared study of photoreaction of ethanol on Au and Ag/TiO_2. Catal. Today. 264, 16–22. DOI: 10.1016/j.cattod.2015.07.038.

32. Jia, Y., Ye, L., Kang, X., You, H., Wang, S. & Yao, J. (2016). Photoelectrocatalytic reduction of perchlorate in aqueous solutions over Ag doped TiO_2 nanotube arrays. Journal of Photochemistry & Photobiology A Chemistry. 328, 225–232. DOI: 10.1016/j.jphotochem.2016.05.023.

33. Karimipour, M., Ebrahimi, M., Abafat, Z. & Molaei, M. (2016). Synthesis of $Ag@TiO_2$ core-shells using a rapid microwave irradiation and study of their nonlinear optical properties. Opt. Mater. 57, 257–263. DOI: 10.1016/j.optmat.2016.05.010.

34. Yao, Y.C., Dai, X.R., Hu, X.Y., Huang, S.Z. & Jin, Z. (2016). Synthesis of Ag-decorated porous TiO_2 nanowires through a sunlight induced reduction method and its enhanced photocatalytic activity. *Appl. Surf. Sci*. 387, 469–476. DOI: 10.1016/j.apsusc.2016.06.130.

35. Spadavecchia, F., Cappelletti, G., Ardizzone, S., Bianchi, C.L., Cappelli, S., Oliva, C., Scardi, P., Leoni, M. & Fermo, P. (2010). Solar photoactivity of nano-n-TiO_2 from tertiary amine: Role of defects and paramagnetic species. *J. Appl. Catal.* 96(3), 314–322. DOI: 10.1016/j.apcatb.2010.02.027.

36. Pawlikowska, M., Fuks, H. & Tomaszewicz, E. (2017). Solid state and combustion synthesis of Mn^{2+} – doped scheelites – their optical and magnetic properties. Ceram. Int. (43)14135–14145. DOI: 10.1016/j.ceramint.2017.07.154.

37. Urbanowicz, P., Piątkowska, M., Sawicki, B., Groń, T., Kukuła, Z. & Tomaszewicz, E. (2015). Dielectric properties of $RE_2W_2O_9$ (RE = Pr, Sm–Gd) ceramics. *J. Eur. Ceram. Soc.* 35(15), 4189–4193. DOI: 10.1016/j.jeurceramsoc.2015.07.028.

38. 36. Zhang, G.Q., Hendrickson, M., Plichta, E.J., Au, M. & Zheng, J.P. (2012). Preparation, Characterization and Electrochemical Catalytic Properties of Hollandite $Ag_2Mn_8O_{16}$ for Li-Air Batteries. *J. Electrochem. Soc.* 159(3), A310–A314. DOI: 10.1149/2.085203jes.

39. Zhang, G., Zheng, J.P., Liang, R., Zhang, C., Wang, B., Au, M., Hendrickson, M. & Plichta, E.J. (2011). Multilayer hollandite $Ag_2Mn_8O_{16}$ catalytic air electrodes for rechargeable lithium-air batteries. Electrode & Catalyst Nanostructures. DOI: 10.1149/1.3655436.

40. Khataee, A., Arefi-Oskoui, S., Fathinia, M., Esmaeili, A., Hanifehpour, Y., Joo, S.W. & Hamnabard, N. (2015). Synthesis, characterization and photocatalytic properties of er-doped PbSe nanoparticles as a visible light-activated photocatalyst. *J. Mol. Catal. A: Chem.* 398, 255–267. DOI: 10.1016/j.molcata.2014.11.009.

41. Hoffmann, M.R., Martin, S.T., Choi, W. & Bahnemann, D.W. (1995). Environmental applications of semiconductor photocatalysis. *J. Chem. Rev.* 95(1), 69–96. DOI: 10.1021/cr00033a004.